Journal of Biomedical Optics

BiomedicalOptics.SPIEDigitalLibrary.org

Ametropia, retinal anatomy, and OCT abnormality patterns in glaucoma. 2. Impacts of optic nerve head parameters

Neda Baniasadi
Mengyu Wang
Hui Wang
Qingying Jin
Tobias Elze

SPIE.

Neda Baniasadi, Mengyu Wang, Hui Wang, Qingying Jin, Tobias Elze, "Ametropia, retinal anatomy, and OCT abnormality patterns in glaucoma. 2. Impacts of optic nerve head parameters," *J. Biomed. Opt.* **22**(12), 121714 (2017), doi: 10.1117/1.JBO.22.12.121714.

Ametropia, retinal anatomy, and OCT abnormality patterns in glaucoma. 2. Impacts of optic nerve head parameters

Neda Baniasadi,[a,b] Mengyu Wang,[a] Hui Wang,[a,c] Qingying Jin,[a,d] and Tobias Elze[a,e,*]
[a]Harvard Medical School, Schepens Eye Research Institute, Department of Ophthalmology, Boston, Massachusetts, United States
[b]University of Massachusetts, Department of Biomedical Engineering and Biotechnology, Lowell, Massachusetts, United States
[c]Jilin University, Department of Psychology, Changchun, Jilin, China
[d]Jilin University of Finance and Economics, Institute for Psychology and Behavior, Changchun, Jilin, China
[e]Max Planck Institute for Mathematics in the Sciences, Leipzig, Germany

Abstract. Clinicians use retinal nerve fiber layer thickness (RNFLT) measured by optical coherence tomography (OCT) as an adjunct to glaucoma diagnosis. Ametropia is accompanied by changes to the optic nerve head (ONH), which may affect how OCT machines mark RNFLT measurements as abnormal. These changes in abnormality patterns may bias glaucoma diagnosis. Here, we investigate the relationship between OCT abnormality patterns and the following ONH-related and ametropia-associated parameters on 421 eyes of glaucoma patients: optic disc tilt and torsion, central retinal vessel trunk location (CRVTL), and nasal and temporal retinal curvature adjacent to ONH, quantified as nasal/temporal slopes of the inner limiting membrane. We applied multivariate logistic regression with abnormality marks as regressands to 40,401 locations of the peripapillary region and generated spatial maps of locations of false positive/negative abnormality marks independent of glaucoma severity. Effects of torsion and temporal slope were negligible. The effect of tilt could be explained by covariation with ametropia. For CRVTL/nasal slope, abnormality pattern shifts at 7.2%/23.5% of the peripapillary region were detected, respectively, independent of glaucoma severity and ametropia. Therefore, CRVTL and nasal curvature should be included in OCT RNFLT norms. Our spatial location maps may aid clinicians to improve diagnostic accuracy. [DOI: 10.1117/1.JBO.22.12.121714]

Keywords: optical coherence tomography; abnormality patterns; refractive error; glaucoma; myopia; optic nerve head.

Paper 170506SSR received Jul. 30, 2017; accepted for publication Dec. 1, 2017; published online Dec. 18, 2017.

1 Introduction

The detection of glaucoma and monitoring the disease progression in patients with myopia are oftentimes challenging.[1] Optic nerve head (ONH) changes and retinal nerve fiber layer (RNFL) thinning in myopic patients may mimic glaucomatous changes.[2] For example, greater cup-to-disc ratio in myopic eyes without the presence of glaucoma can confuse clinicians in differentiating glaucoma from myopic ONH changes.[1,3] Optical coherence tomography (OCT)[4,5] with its capability to image retinal layers at high resolution helps to detect ONH-related small anatomical changes and RNFL thinning and is, therefore, a promising technology to aid clinicians to distinguish ametropia effects from glaucomatous changes of retinal structure. However, despite the widespread adoption of OCT to aid glaucoma diagnosis, the interaction between myopia as a potential confounder or risk factor[6,7] and glaucoma remains complex.[8]

To apply OCT to improve the detection of glaucoma in the presence of axial hyperopia/myopia, it is essential to understand the relationship between RNFL thickness (RNFLT) and ametropia. Previous studies that focused on RNFLT on a single circumpapillary measurement circle around the ONH disagree in their conclusions. While some studies report on thinner RNFL with increasing axial length/myopia,[9–13] which might imply a higher susceptibility of myopes to developing glaucoma, others suggest this effect to be a measurement artifact, because OCT devices do not correct the RNFLT measurement circle for eye size. Increasing axial length implies larger circles, and RNFLT naturally decreases with increasing eccentricity around the ONH. Several studies reported that after correction for axial length-induced magnification effects, correlations between spherical equivalent (SE) of refractive error and RNFLT disappeared, and negative correlations between axial length and RNFLT even tended to become positive after magnification adjustment.[14,15]

The relationship between axial ametropia and RNFLT, however, is location specific and too complex to be fully covered by magnification adjustment. In particular, it has been shown that the two RNFLT peak locations on the measurement circle as well as the corresponding two main temporal retinal nerve fiber bundles are shifted in temporal direction with increasing axial length and/or decreasing SE.[14,16–19] Clinical OCT devices mark locations of abnormally thin RNFL on the measurement printout, and amount and spatial configuration of these abnormality marks are commonly used as an adjunct to clinical glaucoma diagnosis. However, the temporal nerve fiber bundle shifts

*Address all correspondence to: Tobias Elze, E-mail: tobias_elze@meei.harvard.edu

1083-3668/2017/$25.00 © 2017 SPIE

result in substantial and robust shifts of the abnormality patterns regardless of glaucoma severity, as we have shown in a companion paper in the same issue,[19] resulting in considerable areas of fewer or more abnormality ratings for myopes/hyperopes compared to emmetropes, which might bias clinicians and thereby increase false negative as well as false positive glaucoma diagnoses.

These results suggest to routinely determine the trajectories of the main retinal nerve fiber bundles and to calculate individual RNFLT deviations relative to them. However, glaucoma is frequently accompanied by RNFL thinning, which may disguise the predisease locations of the RNFLT peaks in glaucoma patients. Therefore, we and others[19,20] exploited the established finding that circumpapillary RNFLT peak locations are correlated with the locations of the major temporal retinal arteries.[21,22] In our companion paper,[19] we demonstrated that interindividual variations in the interartery angle (IAA), i.e., the angle between the major superior and inferior temporal arteries, account for significant shifts in Cirrus HD-OCT (Carl Zeiss Meditec, Jena, Germany) abnormality ratings at 36.7% of the peripapillary area, compared to 22.9% related to variations in SE. In other words, the potential diagnostic bias introduced by IAA variation is substantially larger than that introduced by ametropia. Moreover, we could show that over 17% of the abnormality rating shifts due to SE are not explained by IAA, which means that ametropia-induced effects are not entirely covariates of IAA induced effects.

Our finding that ametropia effects on OCT RNFLT abnormality profiles are not fully explained by IAA variations[19] suggests that other retinal parameters, which are related to axial ametropia contribute to shifts in abnormality ratings as well. In the current study, we investigate the impact of ONH-related parameters with known associations to ametropia on OCT RNFLT abnormality patterns independent of glaucoma severity.

In a previous work,[23] we systematically studied the relationship between ametropia and a set of ONH-related parameters. Using multivariate regression, we found the following parameters to be significantly and mutually independently related to ametropia: optic disc tilt, optic disc torsion, and the central retinal vessel trunk location (CRVTL) within the ONH. The relationship between abnormality patterns and these parameters, defined below in detail, is investigated in this study. In addition to these parameters directly related to the ONH, another parameter not inside but still in close proximity to the ONH was correlated with SE, namely the average of the nasal and the temporal slope of the retina immediately adjacent to ONH, which we used to define retinal curvature close to ONH. In the present study, we do not consider the average slope but rather the nasal and temporal slopes separately, as we expect different impacts of these two slopes on abnormality patterns.

2 Materials and Methods

This retrospective study was approved by the institutional review board of Massachusetts Eye and Ear (MEE), which waived the need for informed consent. The study adheres to the Declaration of Helsinki.

2.1 *Subjects and Data*

Initially, visual fields (VFs) (Humphrey Field Analyzer HFA-II, Carl Zeiss Meditec, Jena, Germany; protocol: SITA Standard 24–2) and OCT ONH scans (Cirrus HD-OCT, Software version 6.5, Carl Zeiss Meditec AG, Jena, Germany) of all patients measured at the clinical glaucoma practice of MEE between 2011 and 2014 were included if the following criteria were met. The patient had at least one VF with false positive/negative rates $\leq$20% and fixation loss rate $\leq$33% and a Cirrus OCT scan, protocol Optic Disc Cube 200 $\times$ 200, with a signal strength $\geq$6, within one year from the VF measurement. If more than one OCT/VF pair per eye met these criteria, the most recent measurement was selected. If both eyes of a patient matched the criteria, one eye was randomly chosen. In total, OCT/VF measurement pairs of 2161 eyes of 2161 patients fulfilled these initial selection criteria.

2.2 *Data Preprocessing and Reliability Checks*

After the initial selection detailed above, each OCT scan was additionally manually checked for reliability. Details can be found in our companion paper in the same issue.[19] In short, thickness color maps and corresponding fundus images of each eye were centered according to the ONH center, and scans with ONH centers that deviated more than 0.3 mm in vertical or horizontal direction from the fundus image center were excluded, so that an edge of 0.3 mm on each side of the image had to be omitted to ensure data availability for each image pixel over all centered scans.

Fundus images were inspected for eye movement-related artifacts and were excluded if vessel shifts of at least one vessel diameter or visible shifts within the optic disc area were detected. Furthermore, scans with missing data on relevant areas were excluded.

SE of refractive error determined by subjective refraction was not fully available for some patients. Those patients had to be excluded as well. To minimize nonaxial effects of ametropia, patients with visually significant cataract (3+ nuclear sclerosis or worse), pseudophakia, or aphakia were excluded as well.

Apart from these exclusion criteria applied in our companion study, in the present work, we introduced two additional criteria: first, eyes for which the CRVTL could not be identified on the fundus image had to be excluded. Second, as the definition of some of the ONH-related parameters required the analysis of single OCT B-scans (see below), we decided to additionally exclude eyes with diagnosed macular degeneration, since retinal phenomena related to macular diseases, such as drusen, may spread beyond the macular region and thereby interfere with OCT B-scan-related image analyses.

2.3 *ONH-Related Parameters*

ONH border was determined by the Cirrus software as Bruch's membrane opening, and its centroid was defined as ONH center.[24]

Ellipses with three parameters (long axis, short axis, and rotation angle) were fitted to the ONH border, as illustrated in Fig. 1(a), by a nonlinear optimization method.[25] Following our previous study,[23] optic disc "torsion" was defined as the angle between the long axis of the ellipse and the interartery line, which is the center line between the intersection points of the major temporal superior and inferior arteries on the Cirrus standard measurement circle (radius of 1.73 mm around the ONH center). Optic disc "tilt" was defined on the horizontal B-scan closest to the ONH center by a previously introduced method.[23,26,27] In short, nasal and temporal clinical ONH boundaries were marked by a trained observer on the fundus image

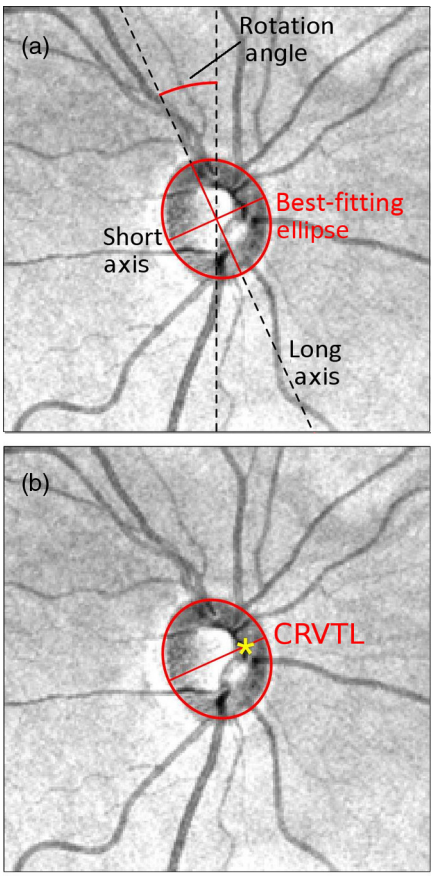

Fig. 1 Illustration of (a) ellipse fitting around ONH and (b) the CRVTL on the short axis of the best-fitting ellipse. For CRVTL tracking, the ellipse was not shown.

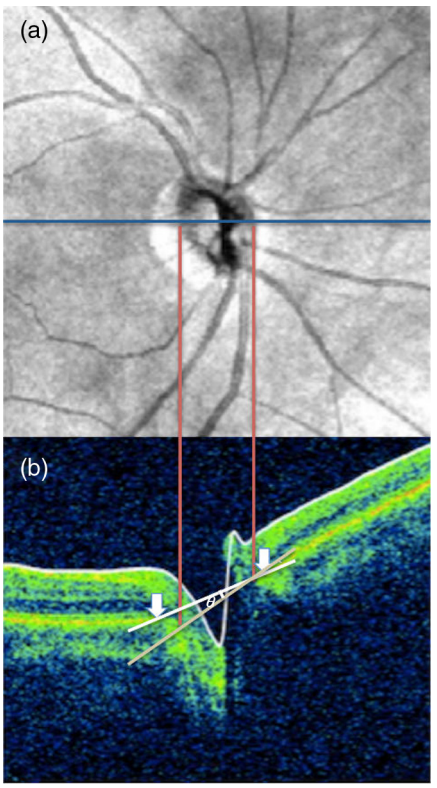

Fig. 2 Illustration of optic disc tilt determination. (a) Step 1: the clinical optic disk boundaries were marked on the horizontal line (blue) through the center of the ONH on the fundus image. The two boundary marks (red lines) were dropped down onto the central horizontal B-scan. (b) Step 2: the inner edges of Bruch's membrane on each side of the ONH (white arrows) were marked on the B-scan and produce a reference plane (white line). The ONH plane was defined by the projection points of the clinical disc margin (red lines). Optic disk tilt (θ) was determined as the angle between reference plane and ONH plane. The figure is reproduced from Ref. 23 published under the Creative Commons license BY-NC-ND 4.0 (https://creativecommons.org/licenses/by-nc-nd/4.0/ accessed on November 21, 2017).

and projected to the respective locations on the central B-scan. The line on the B-scan that connects the ONH boundary projections was defined as the ONH plane. The line between the BMO locations on the central B-scan was used as a reference line, and the tilt angle was defined as the angle between reference line and ONH plane. Figure 2 shows an illustrative example.

The CRVTL, which is the exit point of all retinal blood vessels from the brain inside the ONH, was marked by a trained observer on the short axis of the ellipse, as illustrated in Fig. 1(b). It was normalized, with the temporal pole of the ONH defining location 0 and the nasal pole location 1.

To determine nasal and temporal slopes in proximity to ONH, lines were fitted to nasal and temporal inner limiting membrane, respectively, on the horizontal B-scan closest to ONH center. The fits were performed between the respective image margins and the points at 50 pixels (25% of the image width) temporal and nasal to the ONH center, respectively, as illustrated in Fig. 3.

2.4 *Statistics*

Statistical analyses were performed by the software R (version 3.1.1, R Foundation). To study if or how ONH-related parameters are associated with OCT RNFLT abnormality patterns, we calculated multivariate logistic regression models with the occurrence of abnormality for each of the 40,401 pixels of the Cirrus abnormality images as dependent variables and the respective ONH-related parameter X as one of the regressors. As a second regressor, VF mean deviation (MD) was added (in the following denoted as $X|$MD). MD is an established measure of glaucoma severity, and by analyzing the fitted slope for X in the presence of MD, we ensure that only that part of variance due to X is investigated, which is not explained by glaucoma severity. The specific impacts of the respective regressors were assessed by model comparisons using χ^2 likelihood ratio tests that compare the model with MD as only parameter with the respective model consisting of MD and parameter X. The p values of the 40,401 χ^2 tests for each parameter were adjusted for multiple comparisons by the false discovery rate method.[28] Further descriptions and illustrative examples of this methodology can be found in our companion paper.[19]

As all the parameters are known to be correlated with SE,[23] we additionally calculated all models with SE as a further parameter (in the following denoted by $X|$SE, MD). The respective model comparisons are computed between a model consisting of SE and MD only and a model that adds X as an additional parameter. Thereby, we analyze only that part of the variance of X that is not explained by either glaucoma

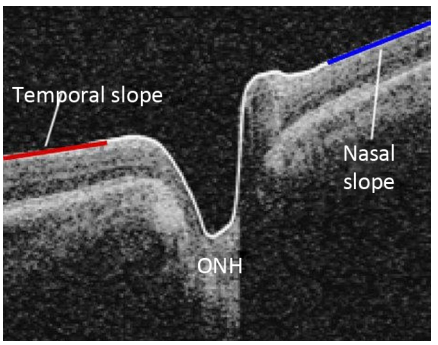

Fig. 3 Illustration of nasal and temporal slope in proximity to the ONH on the horizontal B-scan closest to the ONH center.

severity or ametropia. Finally, as in our companion paper,[19] IAA was identified to have an even stronger impact on abnormality patterns, in an analogous manner, the respective models $X|\text{IAA}, \text{MD}$ were calculated and compared to models consisting of IAA and MD only.

The results are presented as spatial maps of the peripapillary region centered on ONH. For significant slopes of each parameter, the respective image pixel is colored in red or blue, depending on the sign of the slope—the respective meaning of the colors is detailed next to each plot. Otherwise, the pixel is colored in gray.

The definitions of tilt and IAA are composed of several image feature tracking operations by trained observers. As such combinations of subjective judgments might be particularly vulnerable to interobserver judgment differences, we additionally statistically assessed the reproducibility of these two parameters. For 50 randomly chosen eyes from our data set, a second trained observer performed the image feature tracking operations as described above. For these 50 eyes, tilt and IAA derived from the two observers were compared by calculating the "intraclass correlation coefficient (ICC)."[29,30] The ICC denotes the level of agreement between raters and thereby the clinical significance of reproducibility. According to common guidelines,[30,31] an ICC below 0.4 denotes poor agreement between raters, between 0.4 and 0.59 fair agreement, between 0.6 and 0.74 good agreement, and from 0.75 and above excellent agreement.

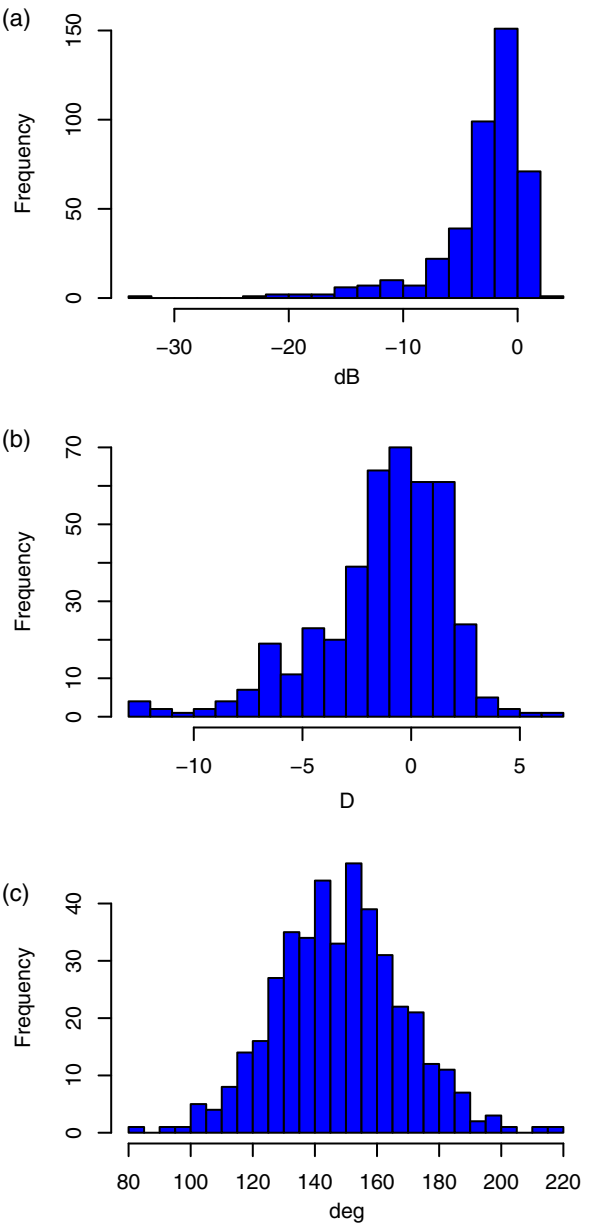

Fig. 4 Histograms of (a) VF MD, (b) SE of refractive error, and (c) IAA of the study participants.

3 Results

1480 of the 2161 eyes were excluded due to OCT quality-related parameters (see Sec. 2). Our companion paper[19] provides the detailed numbers for each exclusion criterion as well as further demographic details about the data set, such as gender and ethnicity. From the remaining 691 eyes, 246 were excluded due to missing SE data and/or cataract. While the remaining 445 eyes have been used in our companion paper, in the present study, 24 further eyes were excluded due to either macular disease and/or the lack of detectability of CRVTL, as detailed in Sec. 2. In total, 421 eyes of 421 participants remained and were included in this study.

The age of the study participants was 58.4 ± 12.9 (mean $\pm$ SD) years (range: 16 to 91 years). Figures 4 and 5 show the histograms of MD (range: −32.4 to 2.01 dB), SE (range: −12.75 to +6.375 D), IAA (range: 85 deg to 219 deg), CRVTL (range: 0.31 to 0.95), nasal slope (range: −0.19 to 2.06), and tilt angle (range: −21.6 deg to 37.1 deg). The reproducibility of tilt and IAA between the two observers, assessed by ICC (see Sec. 2), yielded good agreement for tilt (ICC: 0.67) and excellent agreement for IAA (ICC: 0.99).

Figure 6(a) shows the map with significant shifts in OCT RNFLT abnormality ratings explained by variation of MD alone. The red areas on this map can be interpreted as the locations of significant RNFL thinning with increasing glaucoma severity, which is the case in over 60% of the peripapillary area. This map is a "reference map" for all other maps presented in this work, as the other maps show only the effects of parameter variations that are not explained by variation in MD.

Figures 6(b) and 6(c) show the effects of SE and IAA, respectively, which are not explained by MD. These maps are part of our companion paper as well but have been recalculated here as the number of included eyes has been reduced due to additional

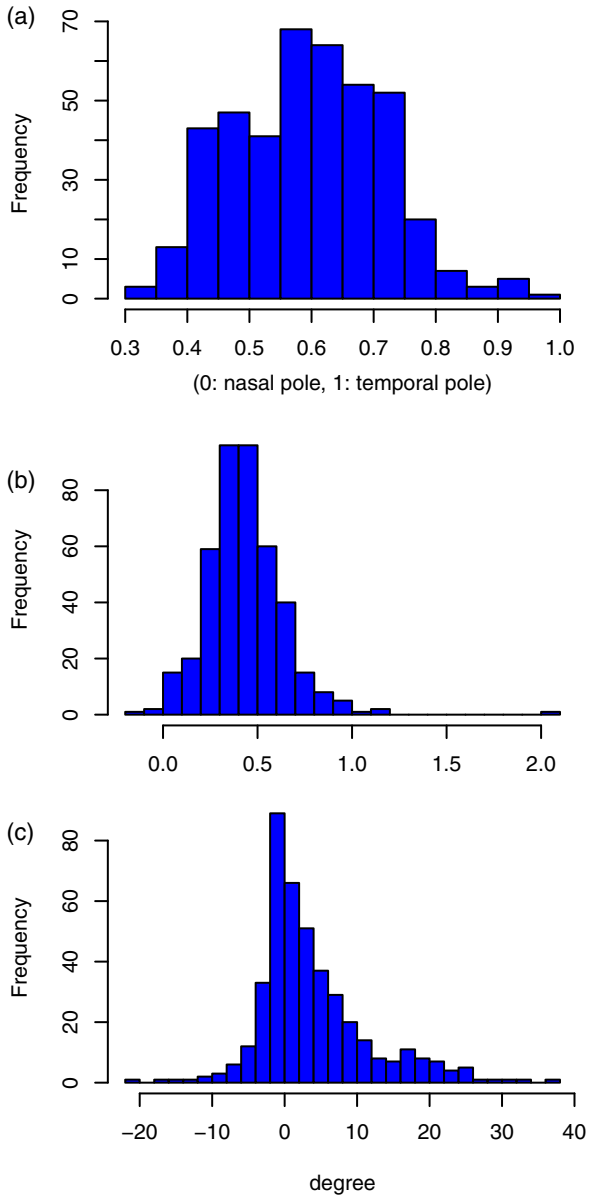

Fig. 5 Histograms of (a) CRVTL, (b) nasal slope, and (c) tilt angle of the study participants.

exclusion criteria. The results are very similar compared to the companion paper and confirm our previous conclusions[19] that SE and IAA account for significant shifts of abnormality ratings on a substantial proportion of the peripapillary area, with considerable areas of increased abnormality ratings (i.e., potential biases toward false positive glaucoma diagnoses) nasal to the median artery locations (magenta squares on the figures) for increasing myopia/decreasing IAA and substantial areas of decreased abnormality ratings (corresponding to potential biases toward false negative diagnoses) in areas temporal to the major arteries for decreasing IAA. In total, 22.5%/38.8% of the peripapillary area are affected for SE/IAA, respectively, as denoted in detail, separately for false positive and false negative cases, on the bottom right of each plot.

For optic disc torsion and temporal slope variation unexplained by MD, less than one percent of the peripapillary area was effected (0.4% and 0.0%, respectively). Given the negligibility of these effects, no maps are shown. The maps for the other three parameters are shown in Figs. 7–9. The respective top right panel shows effects unexplained by MD alone, and the bottom left/right panels effects unexplained by MD and SE/IAA, respectively.

For optic disc tilt variation unexplained by MD, 5.8% of the area is affected [Fig. 7(a)], but these effects are fully explained by covariations with SE and IAA, as the inclusion of these parameters reduces the affected area to 0 [Figs. 7(b) and 7(c)].

For CRVTL variation unexplained by MD [Fig. 8(a)], 19.2% of the area is affected. A part of the area can be explained by covariation with SE, as including SE reduced the affected area to 7.2% [Fig. 8(b)]. The reduction effect for IAA is less strong [10.2% of the area, Fig. 8(c)].

For nasal slope variation (i.e., the local curvature of the retina nasally adjacent to the ONH) unexplained by MD [Fig. 9(a)], 29.8% of the area is affected, with 10.2% of the area subject to increasing abnormality ratings (potential biases toward false positive diagnoses) for nasally "curvier" retinas and 19.6% subject to fewer abnormality ratings (potential biases for false negative diagnoses) for "curvier" retinas, which is equivalent to more abnormality ratings for "flatter" retinas. This effect is particularly concentrated in the nasal area. The areas of fewer abnormality ratings do not decrease with inclusion of SE or IAA and are therefore independent of these parameters. The area of more abnormality ratings decreases to <4% with inclusion of SE or IAA, which suggests substantial covariation effects [Fig. 9(b) and 9(c), respectively].

4 Discussion

For clinicians, OCT RNFLT abnormality ratings are used as an adjunct to the diagnosis of optic neuropathies, such as glaucoma. Clinical ophthalmic OCT devices currently only consider age as a parameter in their normative models. We and others[14,16–19] have demonstrated that ametropia, quantified by SE of refractive error, has a considerable impact on the spatial distribution of RNFLT and that the IAA is a physiological correlate with decisive impact on this spatial distribution. In a companion paper in the same issue,[19] we showed that IAA has a greater impact on shifts in OCT RNFLT abnormality ratings than SE, and at the same time that the SE-related effect was not fully explained by a covariation with IAA. These findings suggested to study the impact of further retinal parameters associated with ametropia.

In a previous work,[23] we quantified the relationships between SE and a set of ONH-related parameters, which had been previously discussed to be either risk factors for glaucoma or confounders for glaucoma diagnosis. Several parameters that were found to be independently associated with SE. In this study, we systematically investigated the impact of these parameters on OCT RNFLT abnormality patterns independent of glaucoma severity. In addition, we studied possible covariation effects between these ONH parameters and SE as well as IAA.

Optic disc torsion and the local retinal curvature temporally adjacent to the ONH, quantified by the local temporal slope of the inner limiting membrane on the central horizontal OCT B-scan, had no or only negligible impacts on abnormality patterns. Optic disc tilt variation independent of glaucoma severity was mildly related to shifts in abnormality ratings, but this impact could be fully explained by covariations with SE and IAA (Fig. 7). In other words, our results suggest that possible OCT RNFLT norms would not need to be adjusted

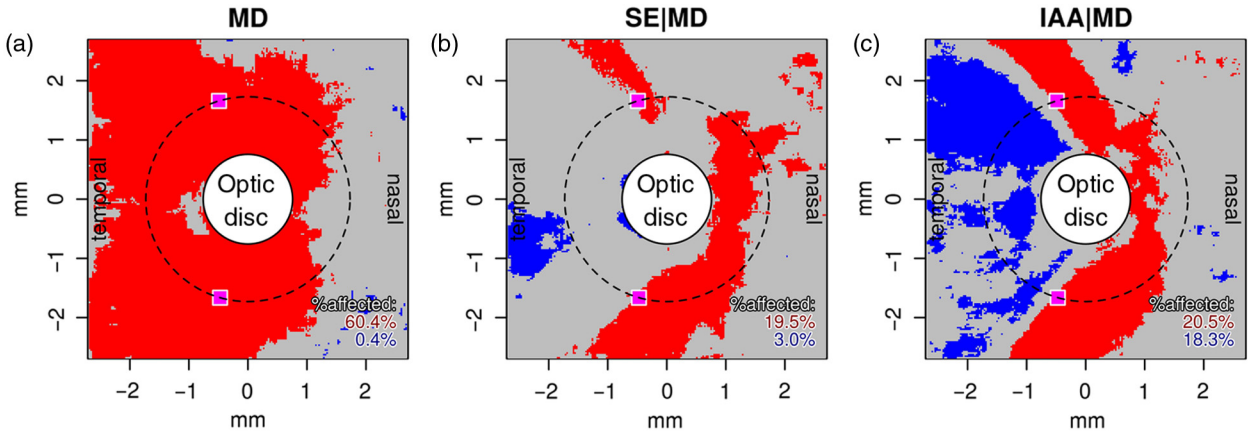

Fig. 6 Maps of peripapillary locations with significant shifts in OCT RNFLT abnormality ratings explained by (a) variation of MD alone, (b) variation of SE unexplained by MD, and (c) variation of IAA unexplained by MD. In (a), red color denotes locations where decreasing MD (i.e., increasing glaucoma severity) is related to an increase in abnormality ratings. In (b), red/blue color denotes more/fewer abnormality ratings for decreasing SE (i.e., increasing myopia). In (c), red/blue color denotes more/fewer abnormality ratings for decreasing IAA. The two magenta squares on each plot denote the median artery locations on the Cirrus standard measurement circle (radius: 1.73 mm, denoted by a stroked line) as a spatial reference.

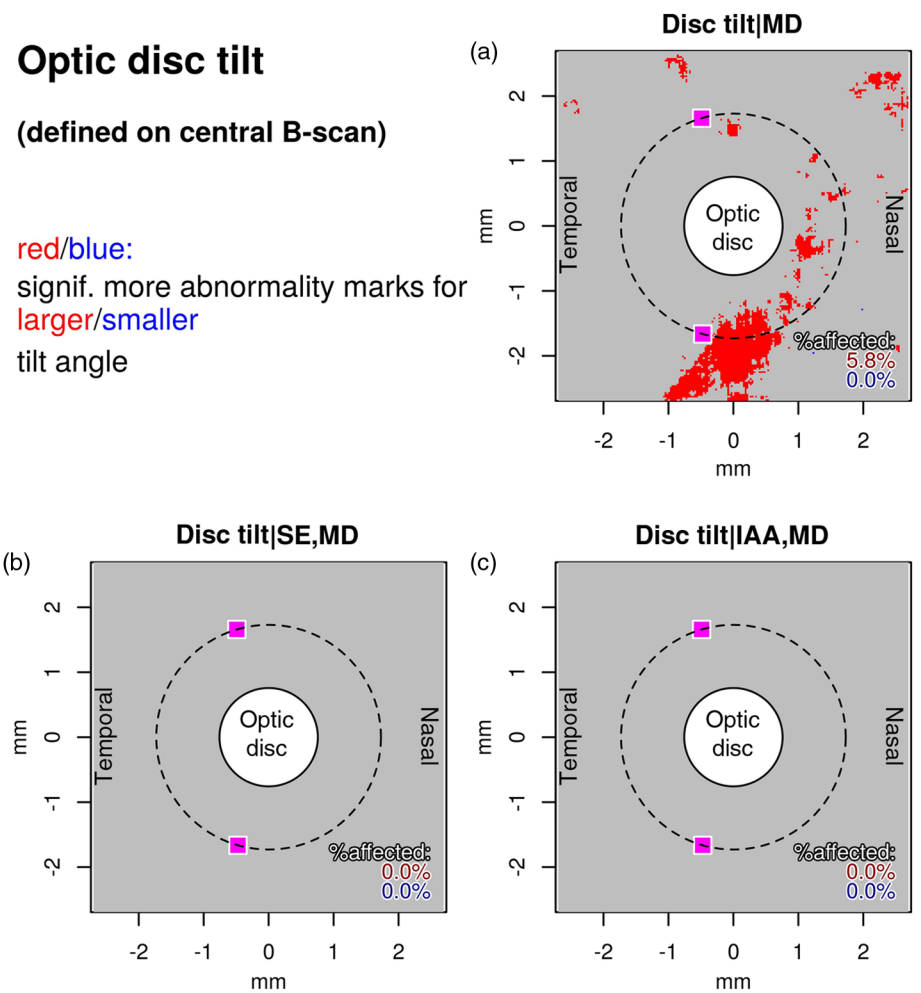

Fig. 7 Map for optic disc tilt effects unexplained by (a) MD, (b) SE and MD, and (c) IAA and MD. The two magenta squares on each plot denote the median artery locations on the Cirrus standard measurement circle (radius: 1.73 mm, denoted by a stroked line) as a spatial reference.

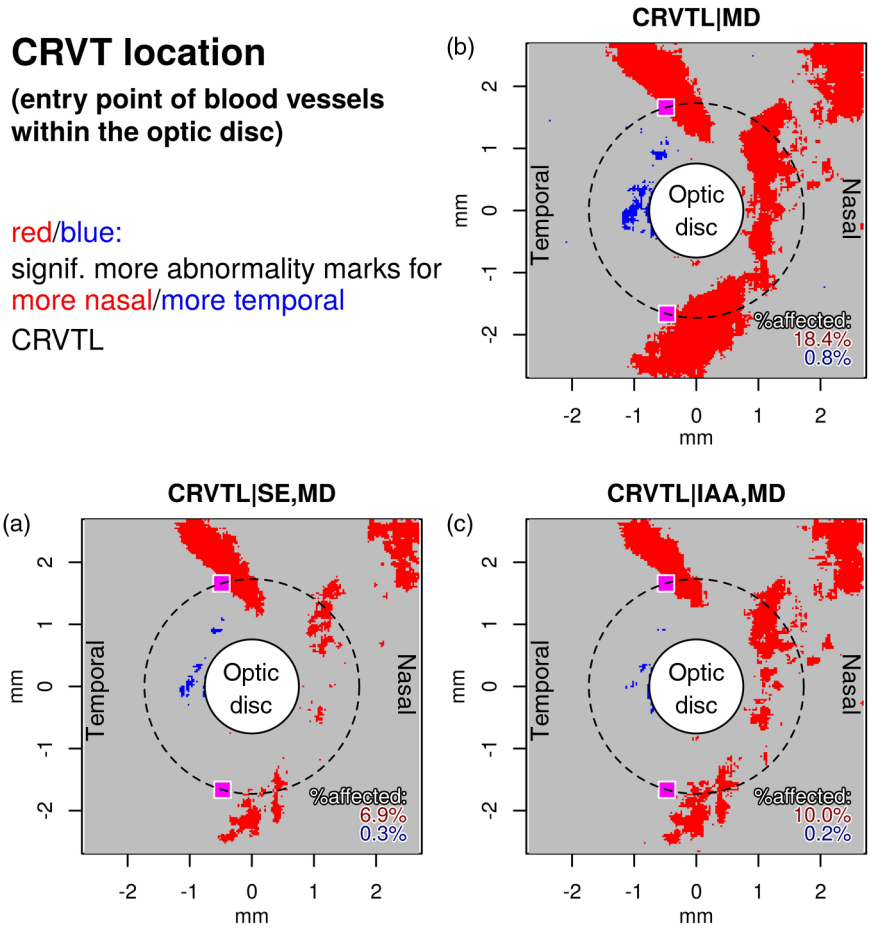

Fig. 8 Map for CRVTL effects unexplained by (a) MD, (b) SE and MD, and (c) IAA and MD. The two magenta squares on each plot denote the median artery locations on the Cirrus standard measurement circle (radius: 1.73 mm, denoted by a stroked line) as a spatial reference.

for tilt provided that either SE or IAA would already have been considered.

The CRVTL has been related to glaucomatous vision loss[32,33] as well as ametropia.[23,34] Here, we demonstrate that CRVTL variation unexplained by glaucoma severity accounts for significant abnormality rating shifts on nearly one fifth of the peripapillary area and that these effects can be partially but not fully explained by covariations with SE or IAA (Fig. 8). Therefore, CRVTL is a potential candidate to be considered for the generation of OCT RNFLT norms.

Variation in the retinal slope nasally adjacent to ONH affects abnormality ratings in two different ways, independent of glaucoma severity. First, steeper slopes are related to more abnormality ratings on retinal areas that resemble the areas of more abnormality ratings with increasing myopia (Fig. 9, red areas). Indeed, these areas can be partially explained by covarations with SE and IAA, as the proportion of red areas in the bottom panels of Fig. 9 is considerably lower than in the top panel. This is in agreement with the previous finding that myopes have more prolate ("curvier") eyes than emmetropes or hyperopes,[35] which implies a steeper slope nasally to ONH. Second, flatter slopes are related to more abnormality marks in the nasal region (Fig. 9, blue areas). This effect is independent of SE and IAA, as the blue areas are not reduced in the bottom panels. The effect is substantial and concerns almost one fifth of the peripapillary area. A likely explanation for the effect is that the OCT device does not rotate curvy retinas before the layer segmentation, i.e., it does not calculate RNFLT perpendicular to the retina, but rather measures layer thickness vertically on the image plane. Increasing rotation of the retina, i.e., steepening of the slope, therefore, necessarily implies a systematic overestimation of RNFLT, with a potential bias of missing true glaucoma. An analogous effect with opposite sign occurs for slopes flatter than average. Retinal curvature naturally increases toward the nasal side, which is a likely explanation that this effect was observed for the nasal but not the temporal slope. Our results suggest that measuring RNFLT perpendicular to the retina instead of vertically on the image plane would substantially improve RNFLT estimations and thereby diagnostic accuracy.

To sum up, our study demonstrates considerable impacts of optic disc tilt, CRVTL, and retinal curvature nasally adjacent to the ONH on OCT RNFLT abnormality patterns. While the effect related to disc tilt could be fully compensated by taking SE or IAA into account, CRVTL and the retinal slope nasally to ONH should be considered additionally to SE and IAA for generating OCT RNFLT norms in future devices. The spatial maps provided by this study may assist ophthalmologists with interpreting RNFLT measurements when diagnosing glaucoma and to compensate biases introduced by specific parameter values.

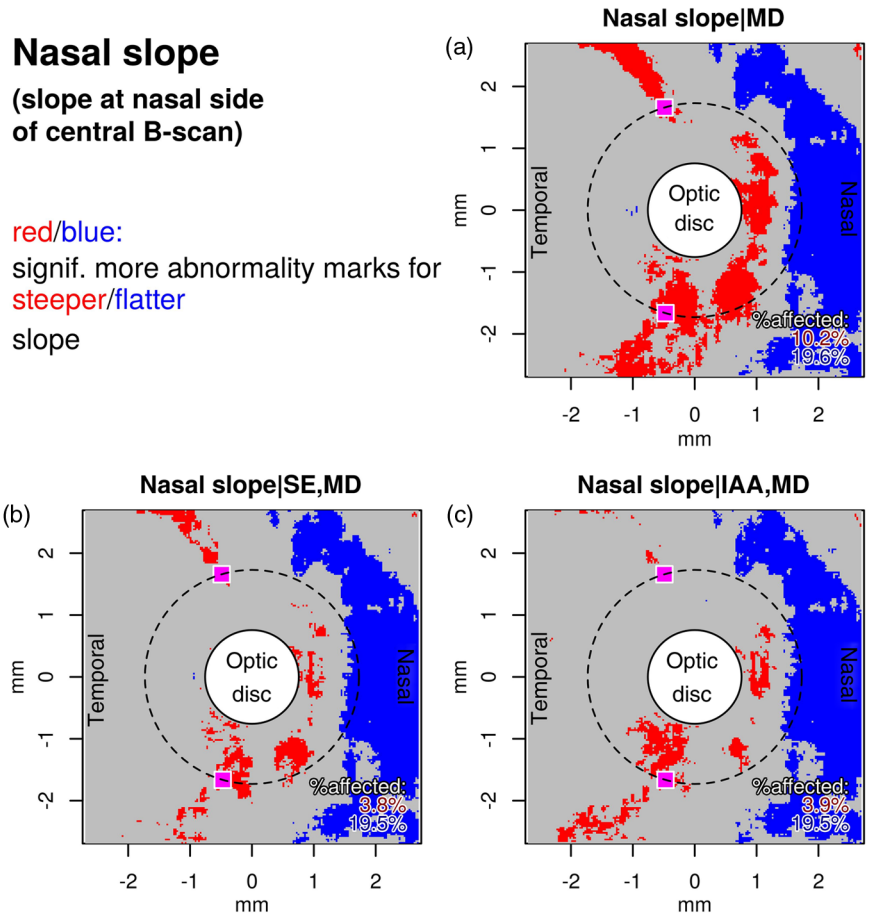

Fig. 9 Map for nasal slope effects unexplained by (a) MD, (b) SE and MD, and (c) IAA and MD. The two magenta squares on each plot denote the median artery locations on the Cirrus standard measurement circle (radius: 1.73 mm, denoted by a stroked line) as a spatial reference.

Disclosures

None of the authors have any conflict of interest to disclose.

Acknowledgments

We wish to thank Dr. Peter J. Bex, Dr. Louis R. Pasquale, Dr. Lucy Q. Shen, Dr. Hiroshi Ishikawa, Dr. Joel Schuman, and Dr. Gadi Wollstein for their collaboration, discussions, and insightful suggestions. This work was supported by the Massachusetts Lions Foundation (T.E., N.B., and M.W.), National Institutes of Health Grant Nos. R01 EY018664 and NEI Core Grant P30EYE003790 (T.E., N.B., M.W.), the Harvard Glaucoma Center of Excellence (T.E.), the China Scholarship Council (Q.J. and H.W.), the BrightFocus Foundation (T.E. and M.W.), and the Research to Prevent Blindness (T.E., N.B., and M.W.).

References

1. J. Y. Lee, K. R. Sung, and S.-C. Yun, "Comparison of rates of retinal nerve fibre layer thinning between patients with non-myopic and myopic glaucoma," *Br. J. Ophthalmol.* **100**(5), 699–703 (2016).
2. R. T. Chang and K. Singh, "Myopia and glaucoma: diagnostic and therapeutic challenges," *Curr. Opin. Ophthalmol.* **24**(2), 96–101 (2013).
3. E. Tay et al., "Optic disk ovality as an index of tilt and its relationship to myopia and perimetry," *Am. J. Ophthalmol.* **139**(2), 247–252 (2005).
4. D. Huang et al., "Optical coherence tomography," *Science* **254**(5035), 1178–1181 (1991).
5. A. A. Aref et al., "Diagnostic specificities of retinal nerve fiber layer, optic nerve head, and macular ganglion cell-inner plexiform layer measurements in myopic eyes," *J. Glaucoma* **23**(8), 487–493 (2014).
6. P. Mitchell et al., "The relationship between glaucoma and myopia: the blue mountains eye study," *Ophthalmology* **106**(10), 2010–2015 (1999).
7. M. W. Marcus et al., "Myopia as a risk factor for open-angle glaucoma: a systematic review and meta-analysis," *Ophthalmology* **118**(10), 1989–1994 (2011).
8. C.-H. Hsu, R. I. Chen, and S. C. Lin, "Myopia and glaucoma: sorting out the difference," *Curr. Opin. Ophthalmol.* **26**(2), 90–95 (2015).
9. C. K.-S. Leung et al., "Retinal nerve fiber layer measurements in myopia: an optical coherence tomography study," *Invest. Ophthalmol. Visual Sci.* **47**(12), 5171–5176 (2006).
10. J. L. Hougaard et al., "Modelling the normal retinal nerve fibre layer thickness as measured by stratus optical coherence tomography," *Graefe's Arch. Clin. Exp. Ophthalmol.* **244**(12), 1607–1614 (2006).
11. D. L. Budenz et al., "Determinants of normal retinal nerve fiber layer thickness measured by stratus OCT," *Ophthalmology* **114**(6), 1046–1052 (2007).
12. F. M. Rauscher et al., "Myopia affects retinal nerve fiber layer measurements as determined by optical coherence tomography," *J. Glaucoma* **18**(7), 501–505 (2009).
13. P. A.-K. M. Salih, "Evaluation of peripapillary retinal nerve fiber layer thickness in myopic eyes by spectral-domain optical coherence tomography," *J. Glaucoma* **21**(1), 41–44 (2012).
14. S. H. Kang et al., "Effect of myopia on the thickness of the retinal nerve fiber layer measured by Cirrus HD optical coherence tomography," *Invest. Ophthalmol. Visual Sci.* **51**(8), 4075–4083 (2010).
15. K. Hirasawa et al., "Determination of axial length requiring adjustment of measured circumpapillary retinal nerve fiber layer thickness for ocular magnification," *PLoS One* **9**(9), e107553 (2014).

16. S. W. Hong et al., "Analysis of peripapillary retinal nerve fiber distribution in normal young adults," *Invest. Ophthalmol. Visual Sci.* **51**(7), 3515–3523 (2010).
17. Y. C. Yoo, C. M. Lee, and J. H. Park, "Changes in peripapillary retinal nerve fiber layer distribution by axial length," *Optom. Vision Sci.* **89**(1), 4–11 (2012).
18. C. K.-S. Leung et al., "Retinal nerve fiber layer imaging with spectral-domain optical coherence tomography: interpreting the RNFL maps in healthy myopic eyes," *Invest. Ophthalmol. Visual Sci.* **53**(11), 7194–7200 (2012).
19. T. Elze et al., "Ametropia, retinal anatomy, and OCT abnormality patterns in glaucoma. 1. Impacts of refractive error and interartery angle," *J. Biomed. Opt.* **22**(12), 121713 (2017).
20. S. Rho et al., "Improvement of diagnostic performance regarding retinal nerve fiber layer defect using shifting of the normative database according to vessel position," *Invest. Ophthalmol. Visual Sci.* **55**(8), 5116–5124 (2014).
21. D. C. Hood et al., "Blood vessel contributions to retinal nerve fiber layer thickness profiles measured with optical coherence tomography," *J. Glaucoma* **17**(7), 519–528 (2008).
22. D. C. Hood et al., "The location of the inferior and superior temporal blood vessels and interindividual variability of the retinal nerve fiber layer thickness," *J. Glaucoma* **19**(3), 158–166 (2010).
23. N. Baniasadi et al., "Associations between optic nerve head related anatomical parameters and refractive error over the full range of glaucoma severity," *Transl. Vision Sci. Technol.* **6**(4), 9 (2017).
24. Carl Zeiss Meditec Inc., *Cirrus HD-OCT User Manual*, Carl Zeiss Meditec Inc., Dublin, California (2012).
25. J. A. Nelder and R. Mead, "A simplex-method for function minimization," *Comput. J.* **7**(4), 308–313 (1965).
26. H. Hosseini et al., "Measurement of the optic disc vertical tilt angle with spectral-domain optical coherence tomography and influencing factors," *Am. J. Ophthalmol.* **156**(4), 737–744 (2013).
27. H.-Y. L. Park et al., "Disc torsion and vertical disc tilt are related to subfoveal scleral thickness in open-angle glaucoma patients with myopia," *Invest. Ophthalmol. Visual Sci.* **56**(8), 4927–4935 (2015).
28. Y. Benjamini and Y. Hochberg, "Controlling the false discovery rate—a practical and powerful approach to multiple testing," *J. R. Stat. Soc. Ser. B–Methodol.* **57**(1), 289–300 (1995).
29. R. L. Ebel, "Estimation of the reliability of ratings," *Psychometrika* **16**(4), 407–424 (1951).
30. J. L. Fleiss, B. Levin, and M. C. Paik, *Statistical Methods for Rates and Proportions*, 3rd ed., John Wiley & Sons, Inc., Hoboken, New Jersey (2003).
31. D. V. Cicchetti, "Guidelines, criteria, and rules of thumb for evaluating normed and standardized assessment instruments in psychology," *Psychol. Assess.* **6**(4), 284–290 (1994).
32. H. Huang et al., "Position of the central retinal vessel trunk and pattern of remaining visual field in advanced glaucoma," *Br. J. Ophthalmol.* **97**(1), 96–100 (2012).
33. M. Wang et al., "Relationship between central retinal vessel trunk location and visual field loss in glaucoma," *Am. J. Ophthalmol.* **176**, 53–60 (2017).
34. T.-W. Kim et al., "Optic disc change with incipient myopia of childhood," *Ophthalmology* **119**(1), 21–26 (2012).
35. D. A. Atchison et al., "Shape of the retinal surface in emmetropia and myopia," *Invest. Ophthalmol. Visual Sci.* **46**(8), 2698–2707 (2005).

Neda Baniasadi is a postdoctoral research fellow in the Ophthalmology Department, Schepens Eye Research Institute/Harvard Medical School. She received her PhD in biomedical engineering and biotechnology from the University of Massachusetts in February 2017 and her MD degree from Tehran University of Medical Sciences in 2009. Her current research interests include applications of optical coherence tomography to the field of ophthalmology especially glaucoma to improve the diagnosis of eye diseases and to monitor their progression over time.

Tobias Elze is an assistant professor of ophthalmology at Harvard Medical School. He received his PhD in computer science from Max Planck Institute for Mathematics in the Sciences in Leipzig, Germany, in 2011. He is the author of more than 20 research papers. His current research interests include applications of optical coherence tomography to the field of ophthalmology in order to improve the diagnosis of eye diseases and to monitor their progression over time.

Biographies for the other authors are not available.